Electronic Supplementary Material (ESI) for Journal of Materials Chemistry A.

Supporting Information

Selectivity and Activity Modulation of Electrocatalytic Carbon Dioxide Reduction by Atomically Dispersed Dual Iron Catalyst

by

Kuan-Chieh Li,[a] Zong-Hua Wu,[a] Chun-Hung Ke,[a] Yao-Chang Lee,[b] Jyh-Fu Lee,[b] Jin-Ming Chen,[b] Shu-Chih Haw,[b] Fu-Te Tsai,[a,*] Wen-Feng Liaw[a,*]

[a]Department of Chemistry and Frontier Research Center of Fundamental and Applied Science of Matters, National Tsing Hua University, Hsinchu 30013, Taiwan

[b]National Synchrotron Radiation Research Center, Hsinchu, Taiwan

E-mail: wfliaw@mx.nthu.edu.tw; fttsai@mx.nthu.edu.tw

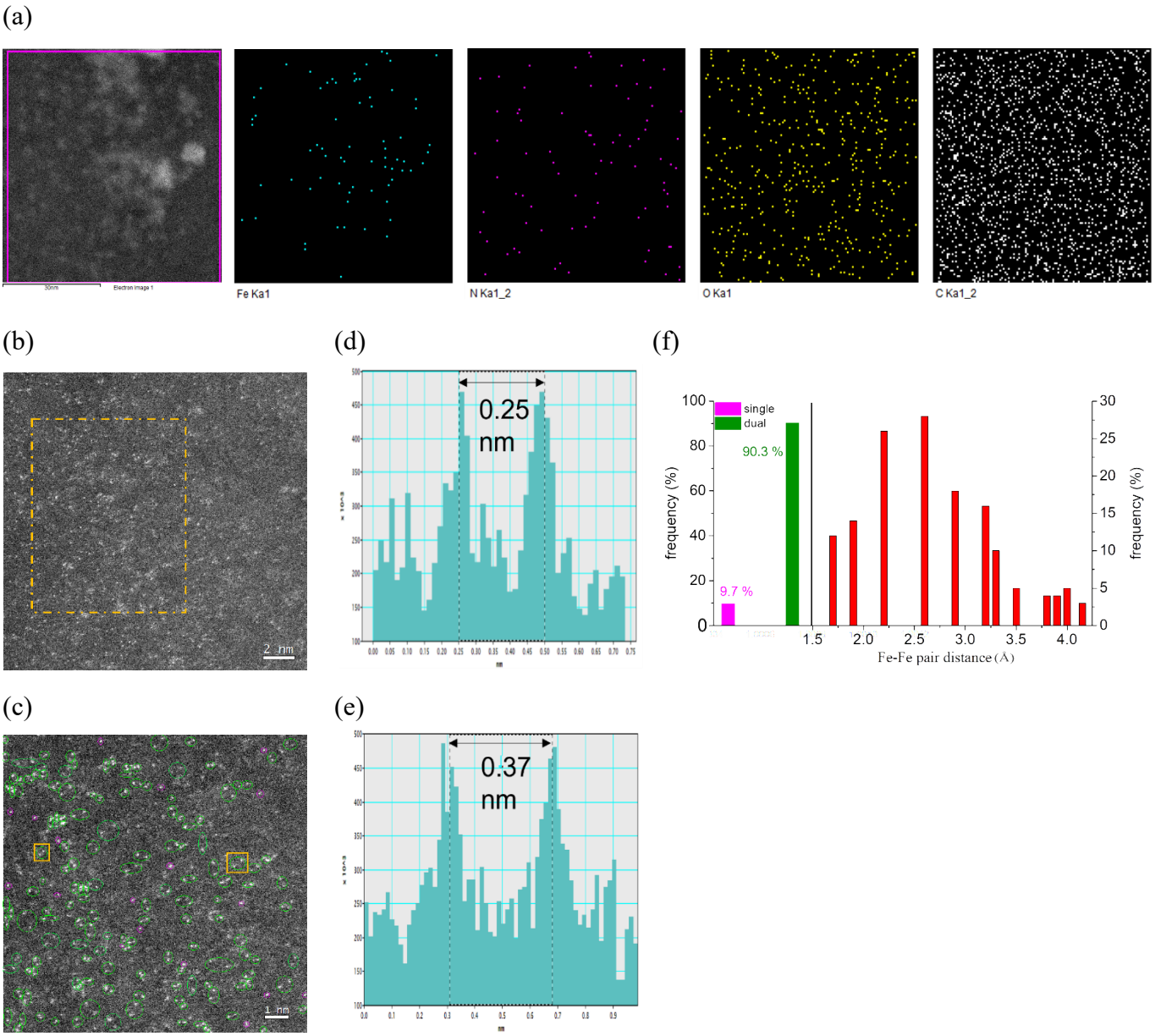

Figure S1. Microscopic characterization of Fe_2/g-C_3N_4 precursor. (a) HAADF-STEM image and corresponding EDX mappings. (b) AC-STEM image. (c) Magnified AC-STEM image. (d)-(e) Intensity profiles gained in the area of yellow squares shown in (c). (f) Statistical density of dual Fe_2 and single Fe sites and Fe-Fe pair distance in (c).

(a)

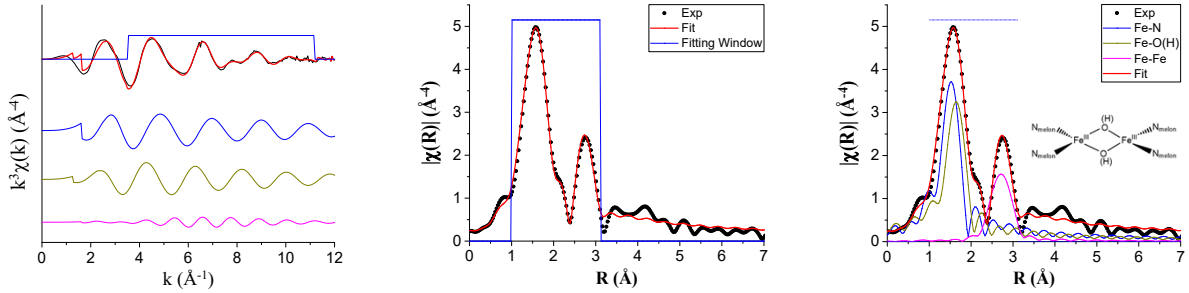

(b)

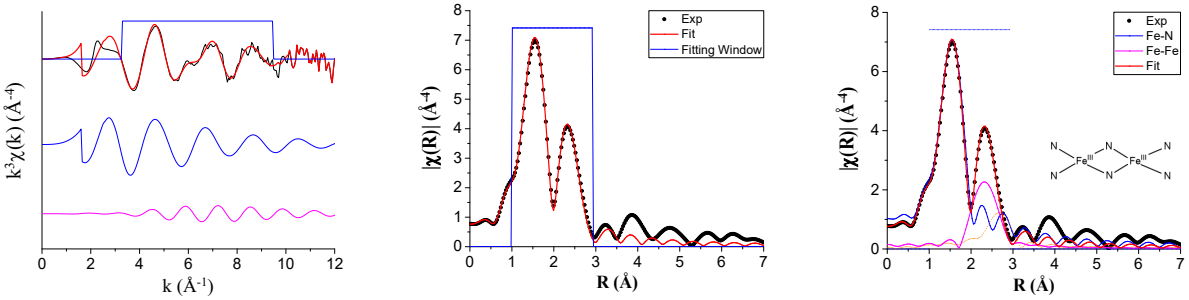

(c)

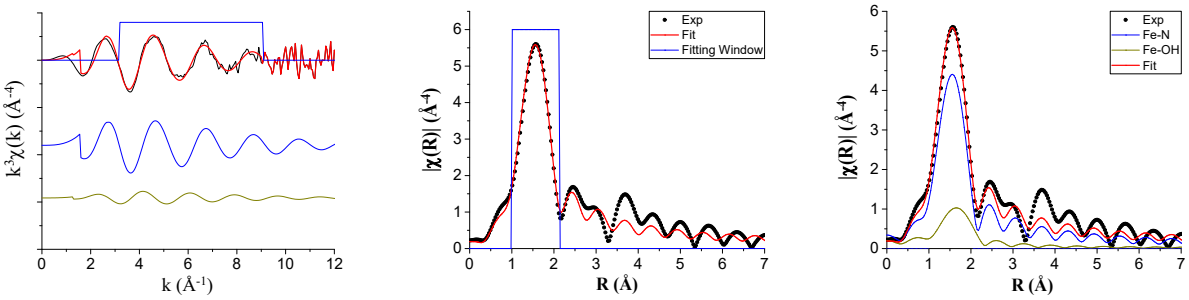

Figure S2. The Fe Kedge k-space and R-space EXAFS spectra of (a) Fe_2/g-C_3N_4 precursor, (b) Fe_2 DAC, and (c) Fe SAC. Shown are data (black) and fitting curves (red) within fitting window (blue), including the deconvoluted path contributions. The detailed EXAFS fitting results are described in Table S1.

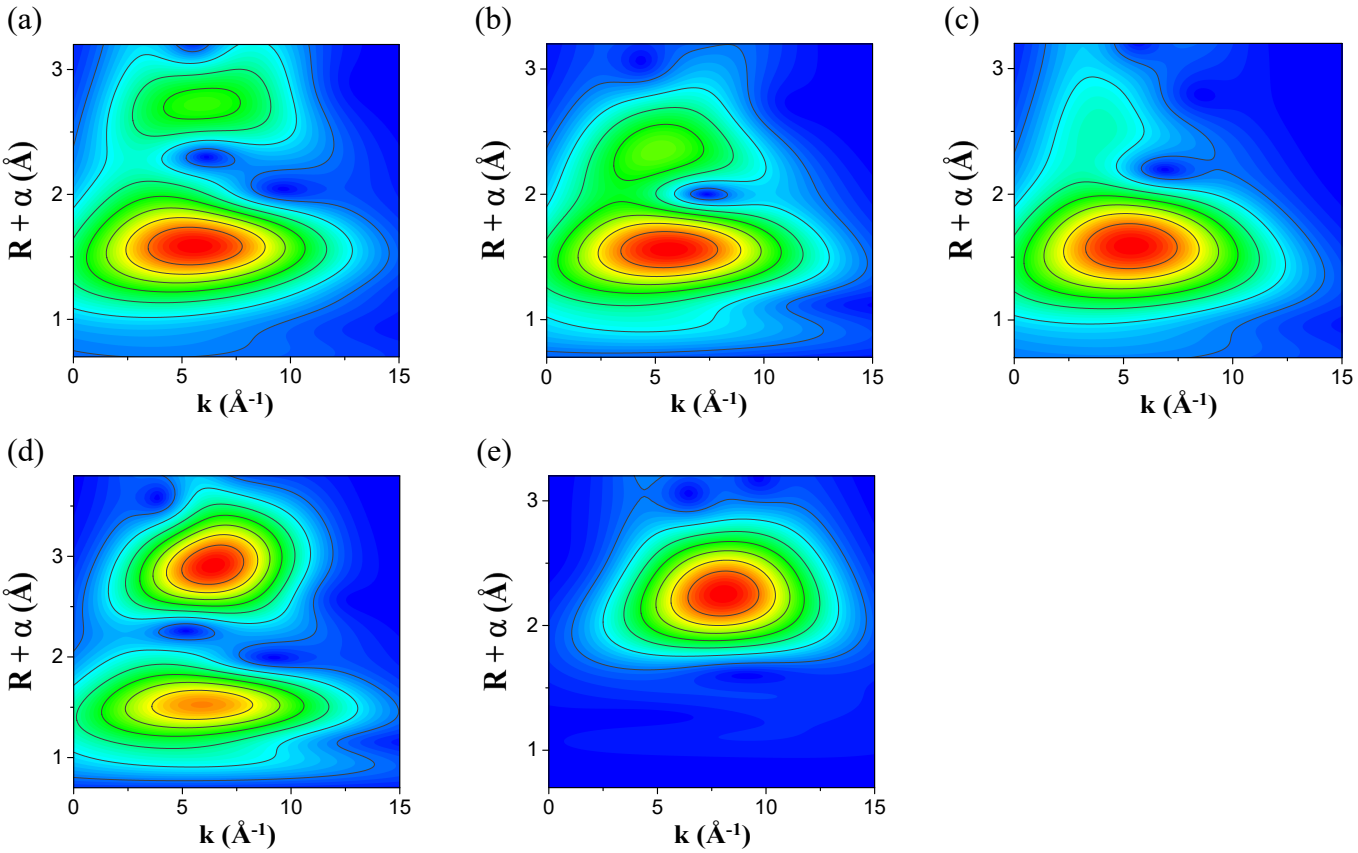

Figure S3. Fe K-edge WT-EXAFS contour plots for (a) Fe_2/g-C_3N_4 precursor, (b) Fe_2 DAC, (c) Fe SAC, (d) Fe_2O_3, and (e) Fe foil.

(a)

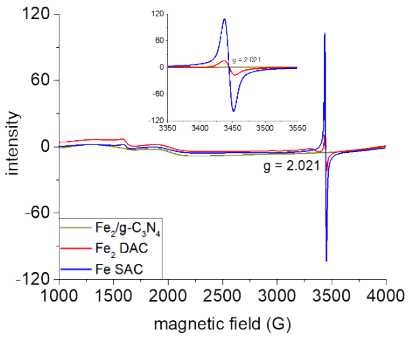

(b)

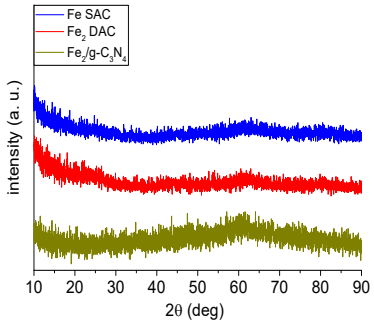

(c)

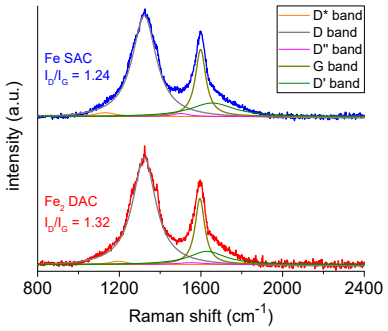

Figure S4. (a) 4 K EPR spectra. (b) pXRD patterns. (c) Raman spectra.[1]

(a)

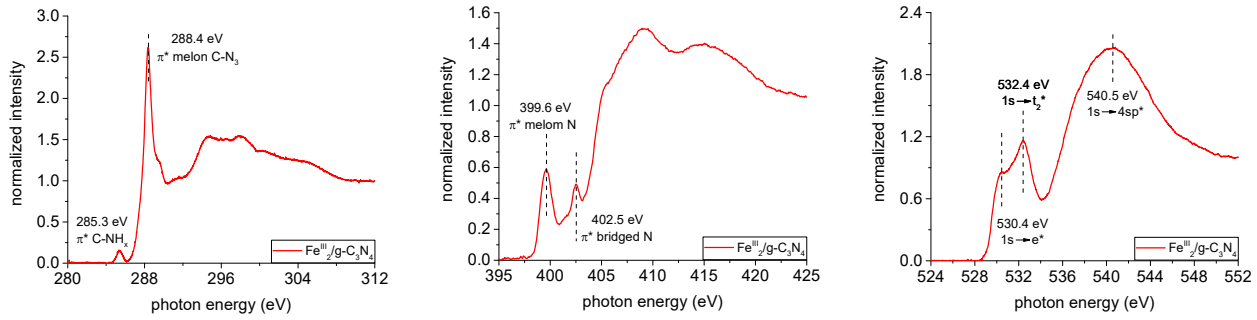

(b)

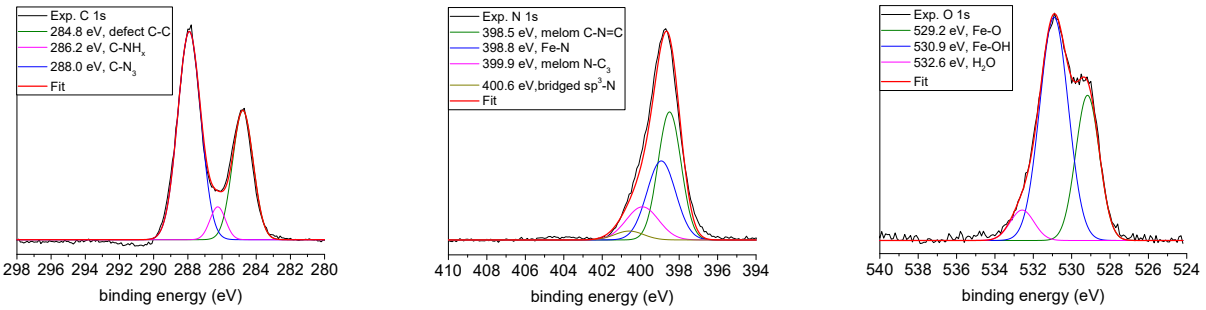

Figure S5. Chemical environment of $Fe_2/g\text{-}C_3N_4$ precursor as probed via (a) soft X-ray absorption spectroscopy, and (b) X-ray photoelectron spectroscopy.

(a)

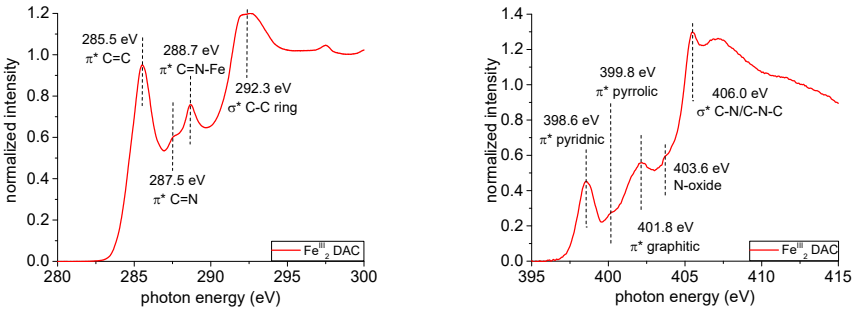

(b)

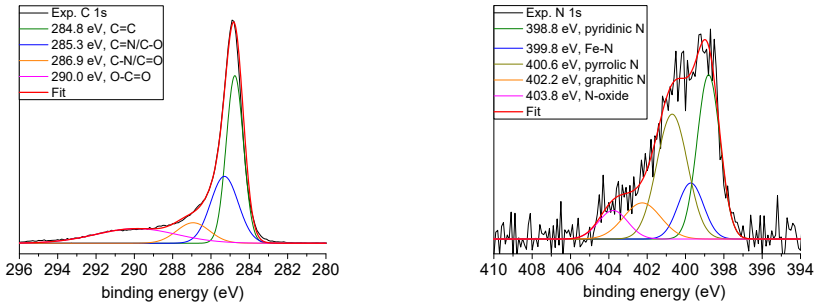

Figure S6. Chemical environment of Fe_2 DAC catalyst as probed via (a) soft X-ray absorption spectroscopy, and (b) X-ray photoelectron spectroscopy.

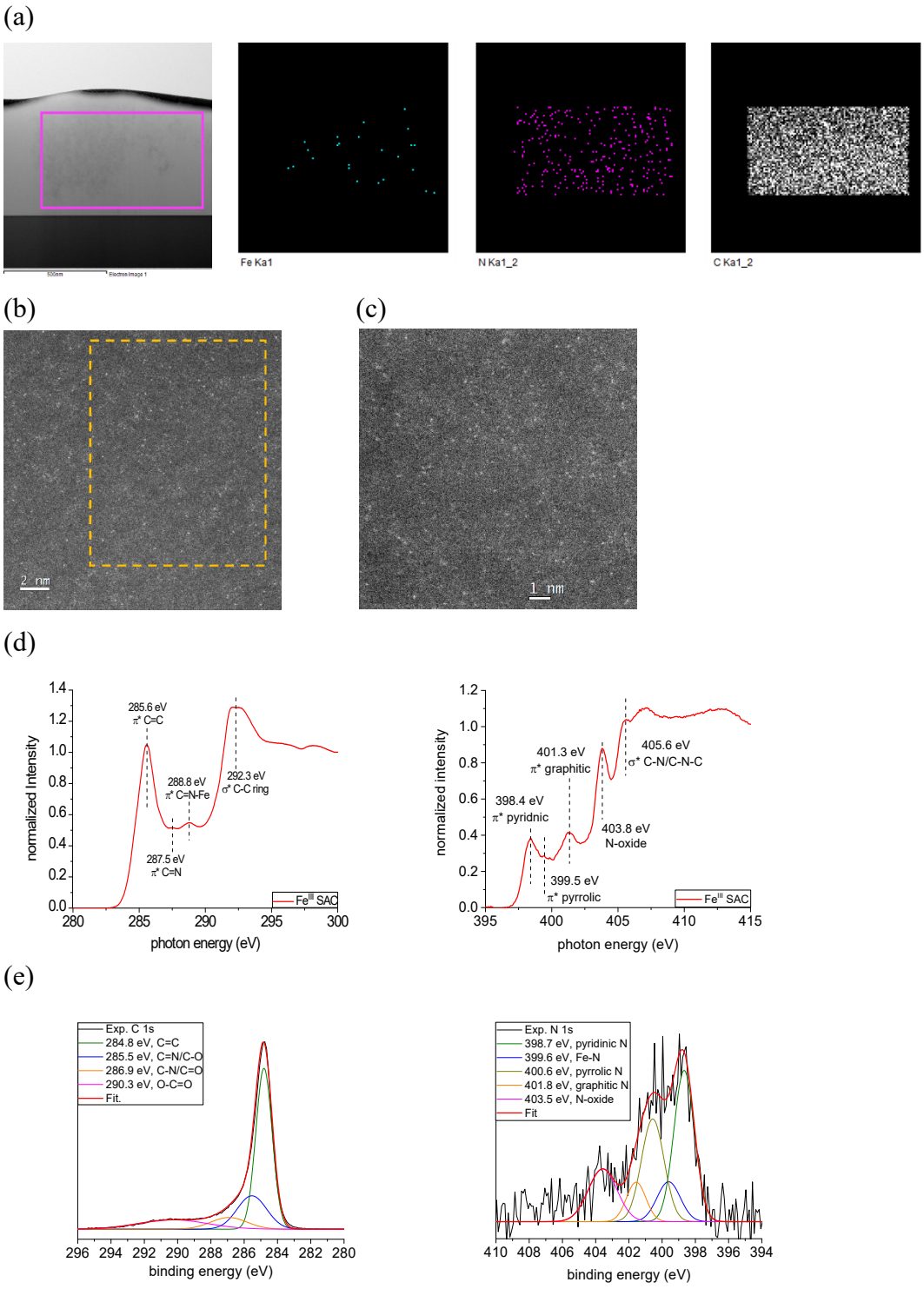

Figure S7. Microscopic characterization of Fe SAC. (a) HAADF-STEM image and corresponding EDX mappings, (b) AC-STEM image, and (c) magnified AC-STEM image. Chemical environment of Fe SAC as probed via (d) soft X-ray absorption spectroscopy, and (e) X-ray photoelectron spectroscopy

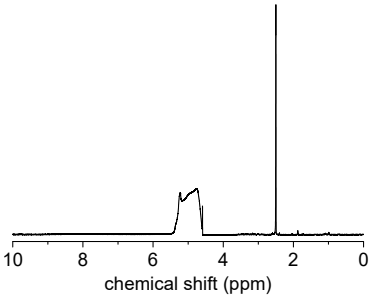

Figure S8. ^{1}H NMR spectrum of liquid sample during electrocatalytic CO_2RR process in CO_2-saturated 0.5 M $KHCO_3$ aqueous solution.

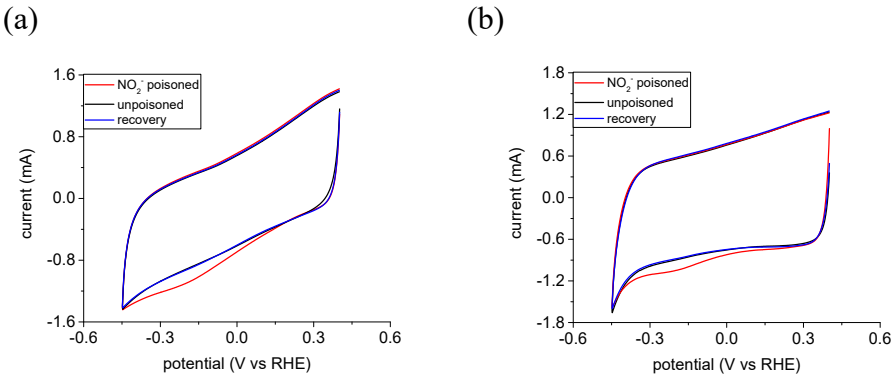

Figure S9. CV curves before (unpoisoned), during (NO_2^- poisoned) and after (recovery) reductive nitrite stripping experiment, used to determine the mole of iron atoms over the surface of (a) Fe_2 DAC and (b) Fe SAC catalytic electrodes in 0.5 M acetate buffer (pH = 5.2).

(a)

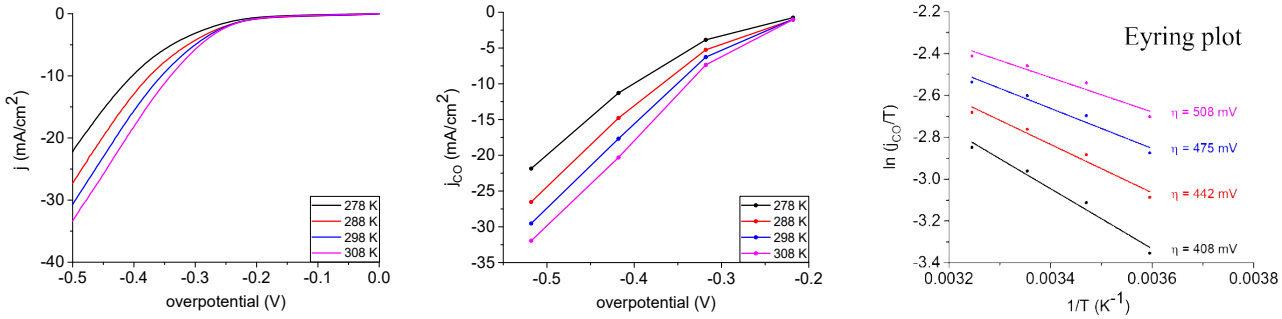

(b)

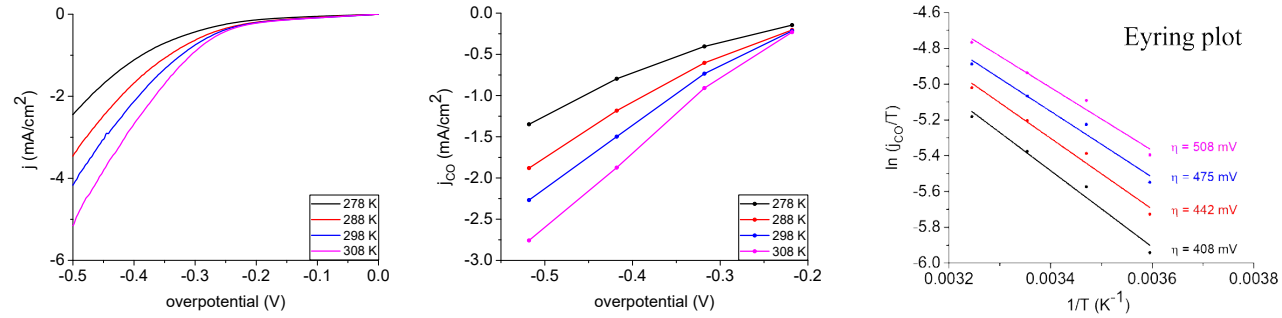

Figure S10. Temperature-dependent kinetic analysis of CO_2RR catalysis on (a) Fe_2 DAC and (b) Fe SAC electrodes in CO_2-saturated 0.5 M $KHCO_3$ aqueous electrolyte.

(a) (b)

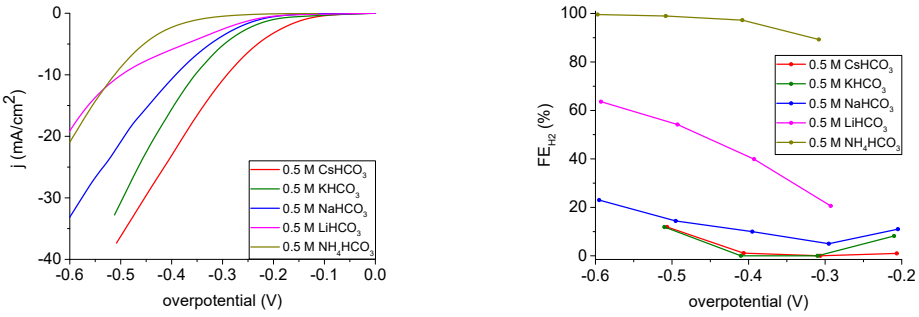

(c) (d)

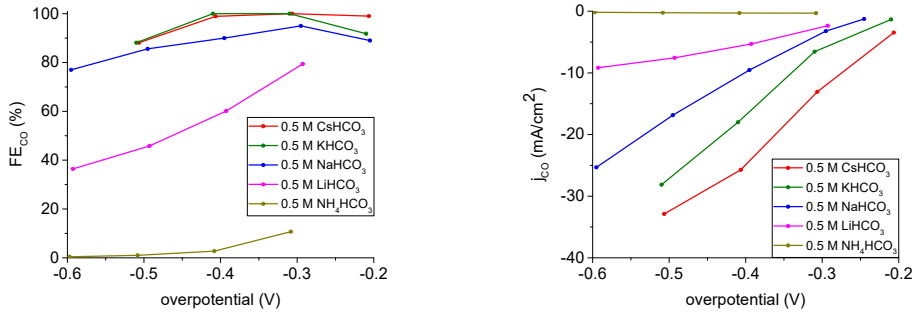

Figure S11. CO_2RR catalytic performance. (a) The LSV curves, (b) H_2 Faradaic efficiency (FE_{H_2}), (c) CO Faradaic efficiency (FE_{CO}), and (d) CO partial current density of Fe_2 DAC electrode in CO_2-saturated 0.5 M $MHCO_3$ aqueous solutions (M = NH_4, Li, Na, K, Cs).

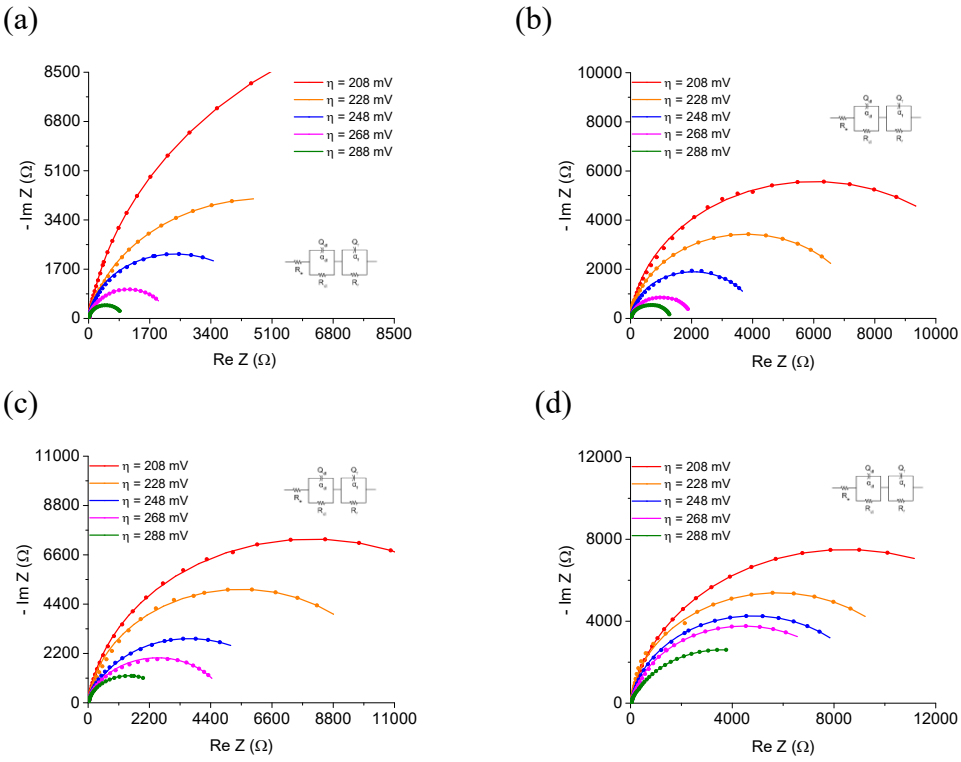

Figure S12. The Nyquist plots of Fe_2 DAC electrode in CO_2-saturated 0.5 M (a) $CsHCO_3$, (b) $KHCO_3$, (c) $NaHCO_3$, and (d) $LiHCO_3$ aqueous solutions.

(a)

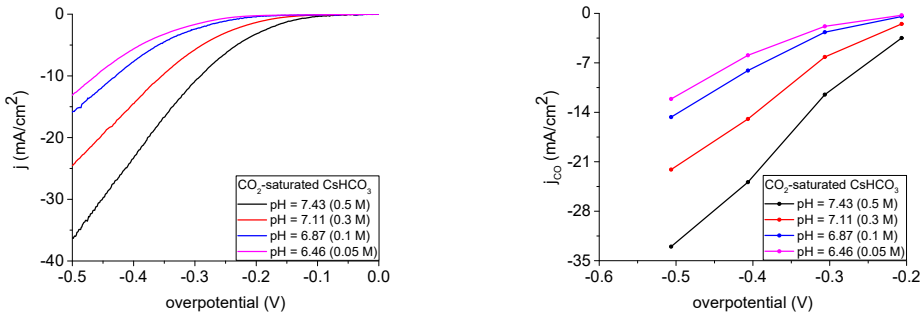

(b)

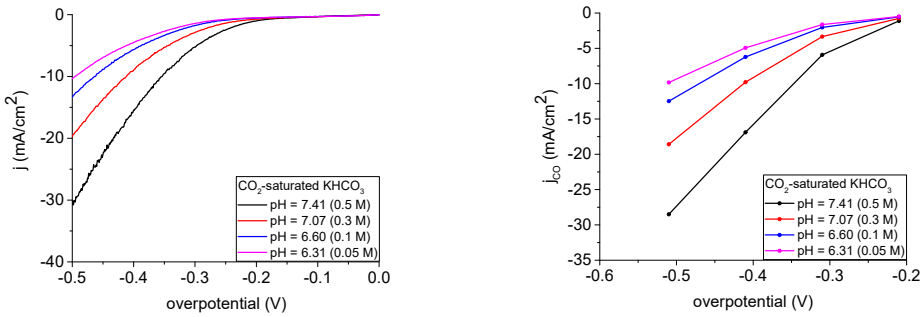

(c)

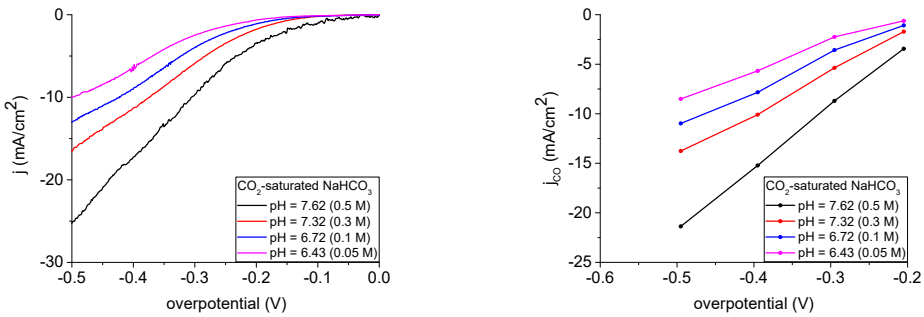

(d)

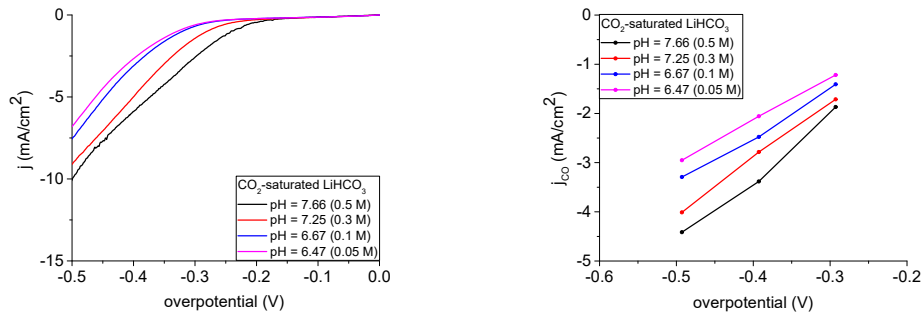

Figure S13. The pH-depedent CO_2RR catalytic behavior of Fe_2 DAC electrode in CO_2-saturated (a) $CsHCO_3$, (b) $KHCO_3$, (c) $NaHCO_3$, and (d) $LiHCO_3$ aqueous solutions.

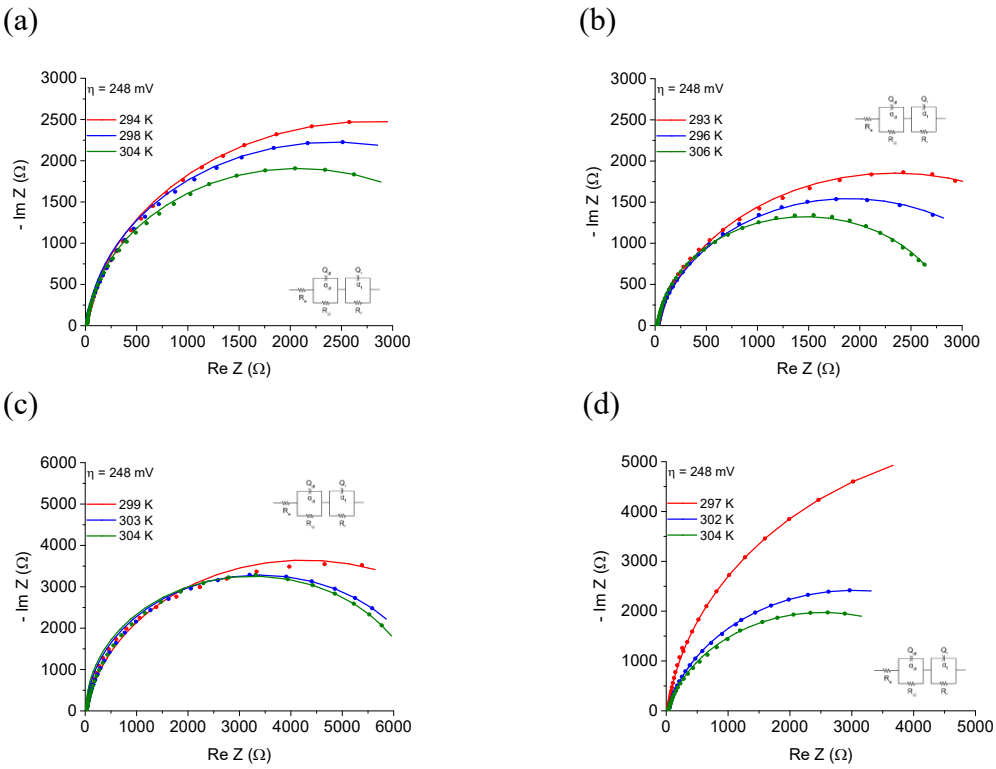

Figure S14. The temperature-dependent Nyquist impedance behaviors of Fe_2 DAC electrode at overpotential of 248 mV in CO_2-saturated 0.5 M (a) $CsHCO_3$, (b) $KHCO_3$, (c) $NaHCO_3$, and (d) $LiHCO_3$ aqueous solutions.

(a)

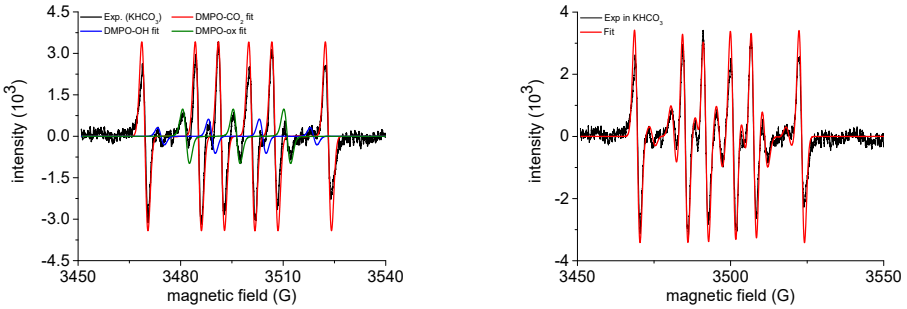

(b)

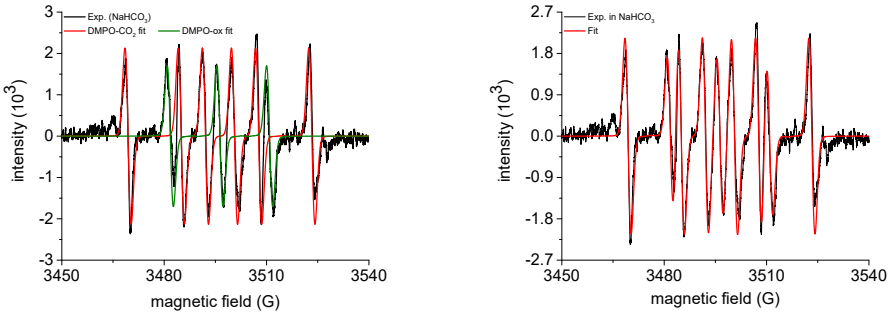

(c)

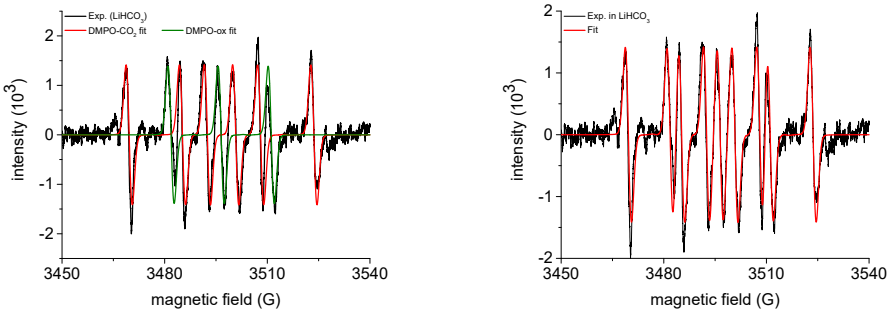

Figure S15. Deconvolution of EPR signal formed in CO_2-saturated 0.1 M (a) $KHCO_3$, (b) $NaHCO_3$, (c) $LiHCO_3$ aqueous solutions, including DMPO-CO_2 (g = 2.0065, a_N = 15.6 G, a_H = 18.9 G), DMPO-OH (g = 2.0065, a_N = 15.1 G, a_H = 15.1 G) and DMPO-oxidized (g = 2.0065, a_N = 14.9 G).

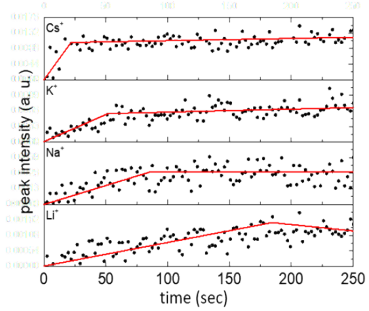

Figure S16. The change in peak intensity of [*COOM]$^-$ (M = Li, Na, K, Cs) intermediate during *operando* ATR-SEIRAS measurements at overpotential of 400 mV.

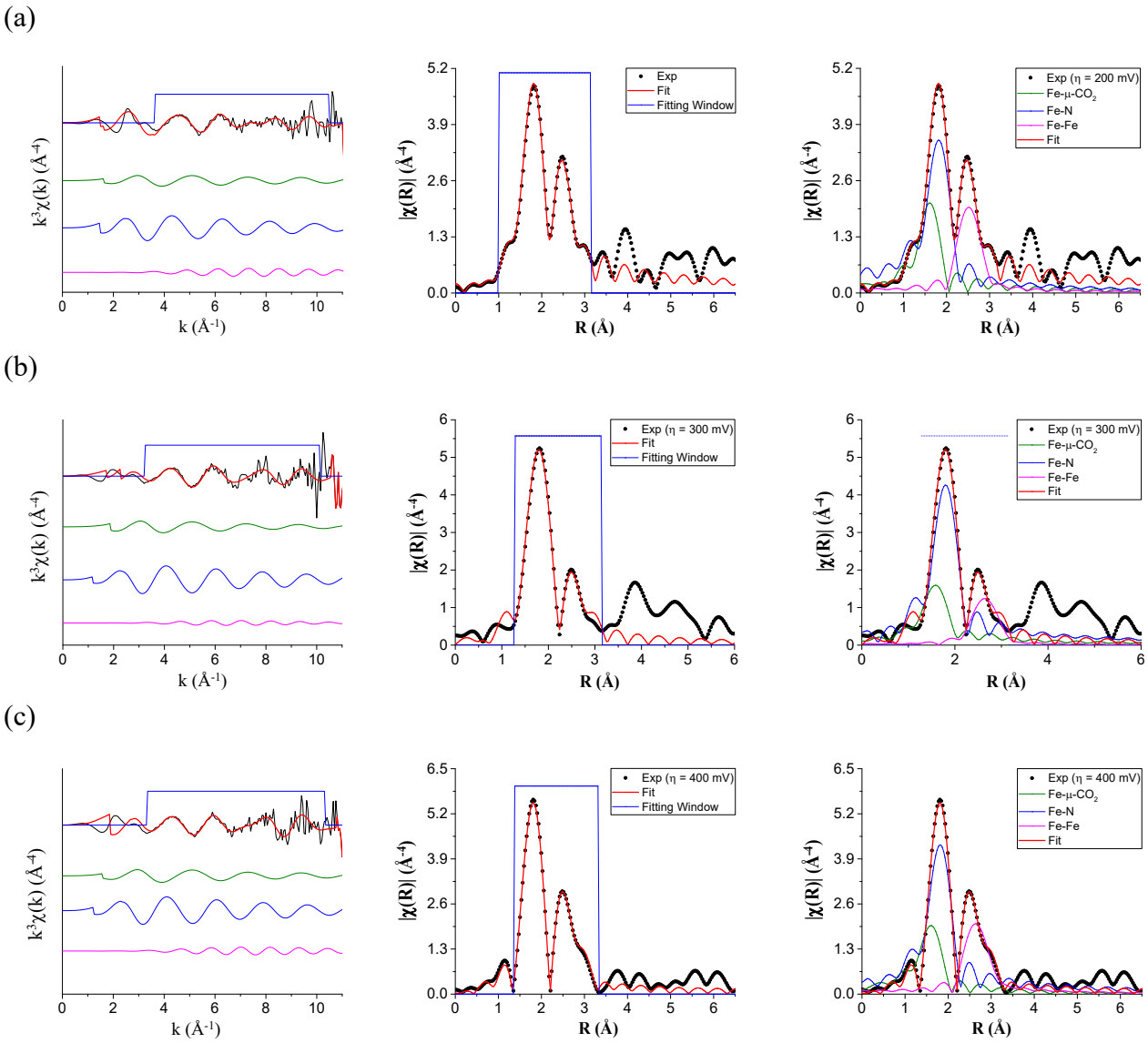

Figure S17. *Operando* Fe K edge k-space and R-space EXAFS spectra of Fe_2 DAC electrode under CO_2RR condition at overpotential of (a) 200 mV, (b) 300 mV, and (c) 400 mV in CO_2-saturated 0.1 M $KHCO_3$ aqueous solution. Shown are data (black) and fitting curves (red) within fitting window (blue), including the deconvoluted path contributions. The detailed EXAFS fitting results are described in Table S2.

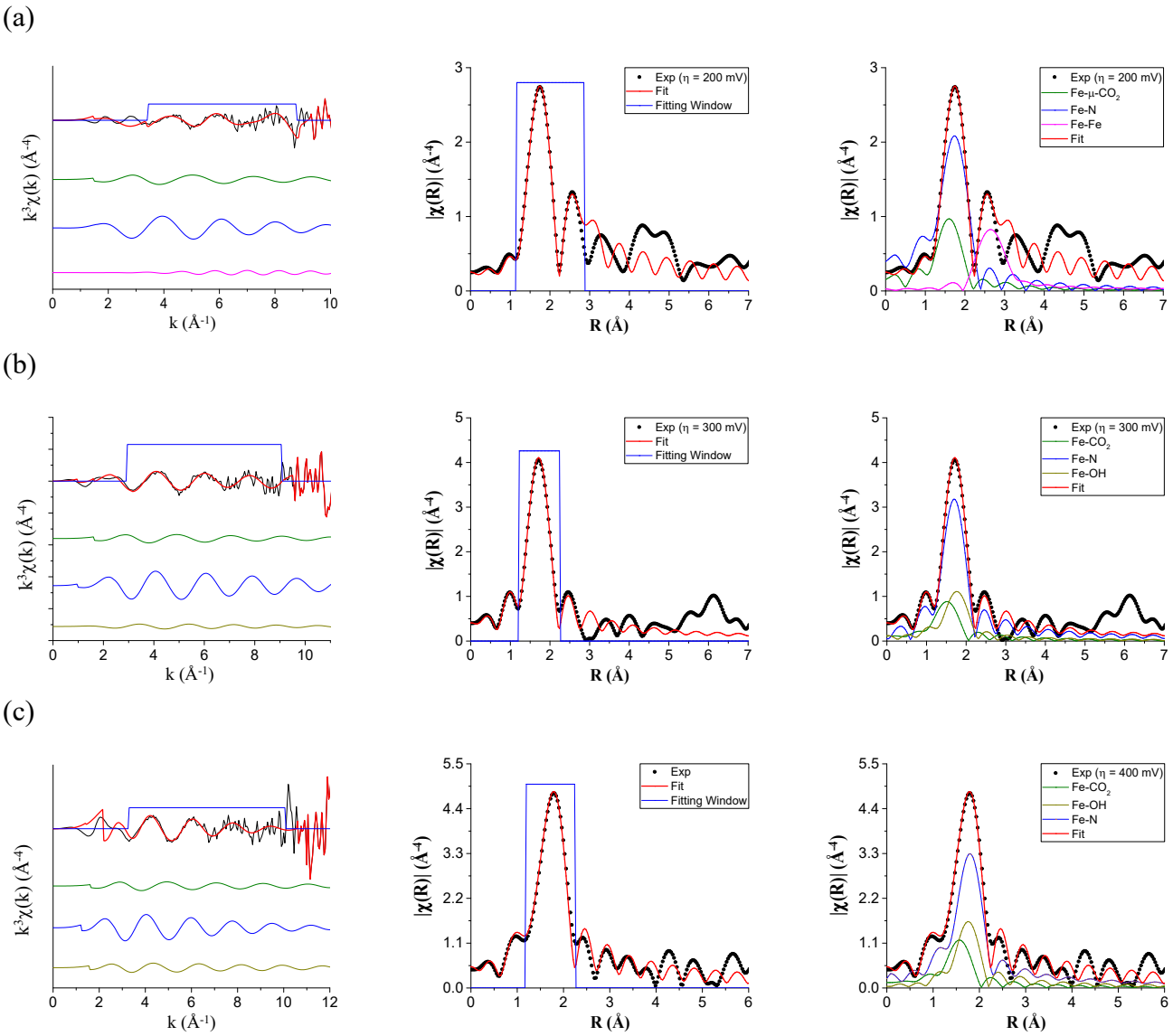

Figure S18. *Operando* Fe K edge k-space and R-space EXAFS spectra of Fe_2 DAC electrode under CO_2RR condition at overpotential of (a) 200 mV, (b) 300 mV, and (c) 400 mV in CO_2-saturated 0.1 M $LiHCO_3$ aqueous solution. Shown are data (black) and fitting curves (red) within fitting window (blue), including the deconvoluted path contributions. The detailed EXAFS fitting results are described in Table S3.

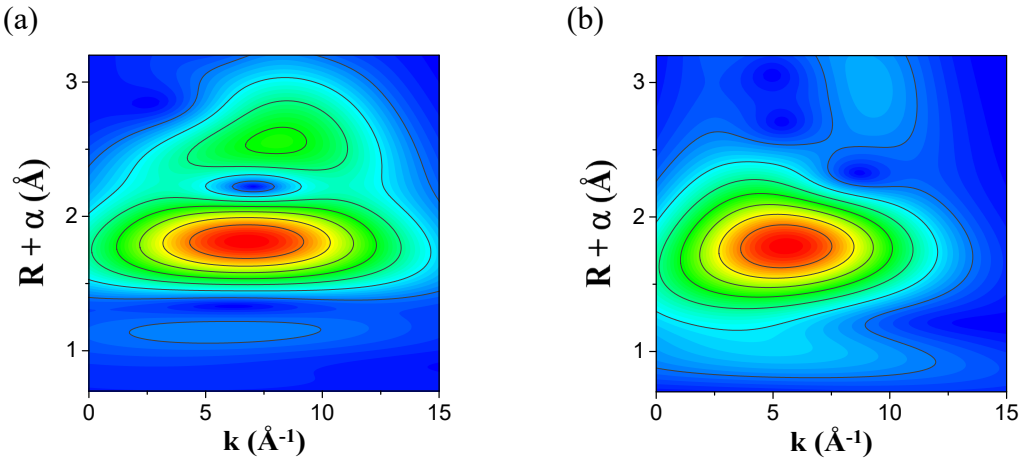

Figure S19. Fe K-edge WT-EXAFS contour plots of Fe_2 DAC electrode in CO_2-saturated (a) 0.1 M $KHCO_3$ and (b) 0.1 M $LiHCO_3$ solution at overpotential of 400 mV.

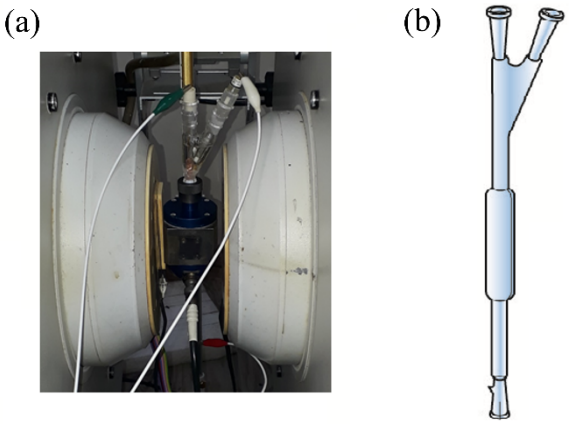

Figure S20. (a) In operando EPR measurement setup and (b) image of the Suprasil flat quartz cell.

(a)

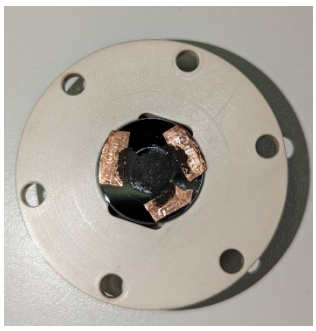

(b)

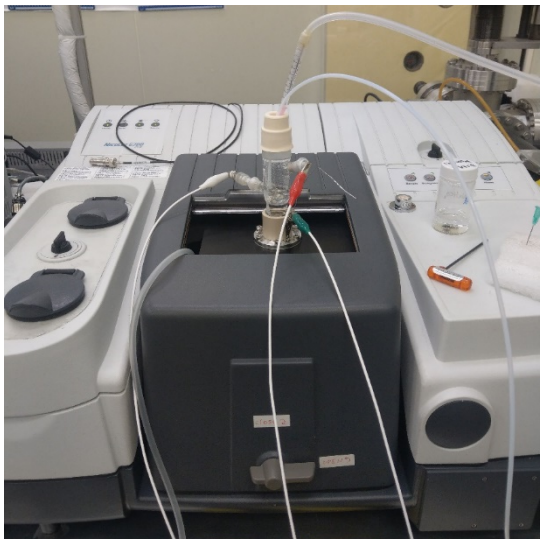

Figure S21. (a) Fe_2 DAC catalyst deposited on the fresh surface (Si prism) with three small pieces of conductive copper tapes and (b) In operando ATR-SEIRAS measurement setup.

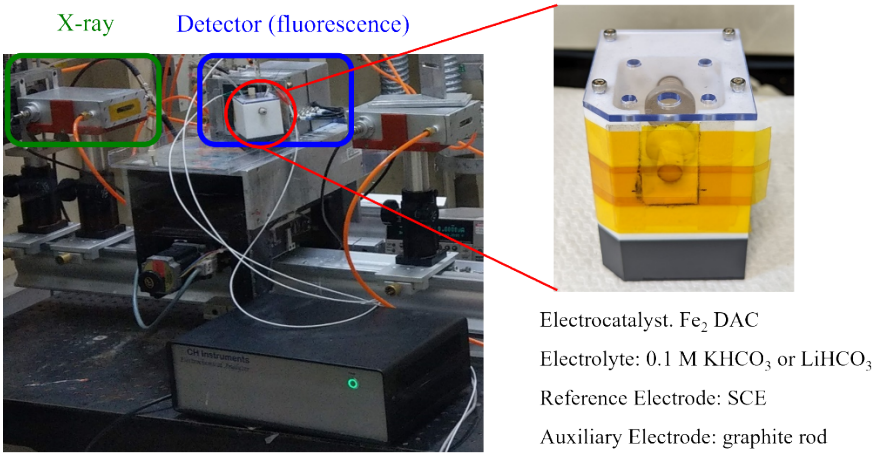

Figure S22. (a) In operando Fe K-edge XAS measurement setup and the customized operando electrochemical cell.

Table S1. Multi-path EXAFS fitting results for Fe_2/g-C_3N_4, Fe_2 DAC and Fe SAC material models. Amplitude reduction factor (S_0^2) was fixed at 0.9.

material models		Fe_2/g-C_3N_4	Fe_2 DAC	Fe SAC
Fe-N path	C.N.	2.23	4.47	4.48
	R (Å)	1.91	1.98	1.98
	ΔE_0 (eV)	9.924	9.971	9.659
	σ^2 (10^{-3}xÅ^2)	3.25	7.73	7.04
Fe-Fe path	C.N.	1.12	1.19	
	R (Å)	3.01	2.71	
	ΔE_0 (eV)	9.889	0.717	
	σ^2 (10^{-3}xÅ^2)	9.85	7.77	
Fe-O(H) path	C. N.	2.30		1.18
	R (Å)	2.03		2.09
	ΔE_0 (eV)	5.928		6.400
	σ^2 (10^{-3}xÅ^2)	4.13		7.71
R factor		0.00382	0.00498	0.00081

Table S2. Multi-path EXAFS fitting results for Fe_2 DAC electrode under CO_2RR operational condition at overpotentials from 200 to 400 mV in CO_2-saturated 0.1 M $KHCO_3$ aqueous electrolyte. Amplitude reduction factor (S_0^2) was fixed at 0.9.

overpotenials		200 mV	300 mV	400 mV
Fe-CO_2 path	C.N.	1.19	1.14	1.18
	R (Å)	1.85	1.86	1.85
	ΔE_0 (eV)	9.975	9.977	9.705
	σ^2 (10^{-3}xÅ^2)	3.01	4.97	4.74
Fe-N path	C.N.	4.03	4.21	4.05
	R (Å)	2.08	2.13	2.13
	ΔE_0 (eV)	7.873	3.650	5.783
	σ^2 (10^{-3}xÅ^2)	5.10	5.11	5.14
Fe-Fe path	C. N.	1.16	1.11	1.13
	R (Å)	3.04	3.14	3.14
	ΔE_0 (eV)	-9.589	-9.988	-9.988
	σ^2 (10^{-3}xÅ^2)	5.17	9.97	5.60
R factor		0.00438	0.00759	0.00509

Table S3. Multi-path EXAFS fitting results for Fe_2 DAC electrode under CO_2RR operational condition at overpotentials from 200 to 400 mV in CO_2-saturated 0.1 M $LiHCO_3$ aqueous electrolyte. Amplitude reduction factor (S_0^2) was fixed at 0.9.

overpotenials		200 mV	300 mV	400 mV
Fe-CO_2 path	C.N.	0.83	0.77	0.61
	R (Å)	1.88	1.90	1.91
	ΔE_0 (eV)	7.892	9.934	9.861
	σ^2 (10^{-3}xÅ^2)	3.01	3.83	3.03
Fe-N path	C.N.	4.42	4.48	4.44
	R (Å)	2.07	2.12	2.15
	ΔE_0 (eV)	-5.041	3.457	6.298
	σ^2 (10^{-3}xÅ^2)	7.39	4.43	8.00
Fe-Fe path	C. N.	0.76		
	R (Å)	3.15		
	ΔE_0 (eV)	-9.957		
	σ^2 (10^{-3}xÅ^2)	7.42		
Fe-O(H) path	C. N.		1.08	1.11
	R (Å)		2.05	2.07
	ΔE_0 (eV)		-5.664	9.948
	σ^2 (10^{-3}xÅ^2)		6.06	3.64
R factor		0.00815	0.00551	0.00624

Reference

1 A. Y. Lee, K. Yang, N. D. Anh, C. Park, S. M. Lee, T. G. Lee and M. S. Jeong, *Appl. Surf. Sci.*, 2021, **536**, 147990.